Transient Field Produced by a Traveling-Wave Wire Antenna

Edward J. Rothwell, *Member, IEEE*, Michael J. Cloud, *Member, IEEE*, and Ponniah Ilavarasan

Abstract—**The electromagnetic fields of a transient traveling wave current on a straight wire segment are calculated directly in the time domain. Retarded potential theory is used to establish an impulse response valid in both far and near zones. A closed-form expression for the field due to a rectangular current pulse is obtained, and corresponding plots are given. Comparison with experimental data reveals close agreement. A formula for far-zone radiation from an arbitrarily shaped wire is developed; results for a proposed directive antenna geometry are presented.**

I. Introduction

TRANSIENT fields produced by traveling-wave currents on linear antennas have become an increasingly important research topic [1-7]. Most work (see, for example, [8]) is done in the frequency domain with transform techniques. Although this type of approach gives accurate solutions, it seems to obscure the physical pictures available in a purely time-domain analysis.

In this paper, the time-domain impulse response of a straight wire supporting a traveling-wave current is obtained via a potential theory, and the superposition concept yields an expression for general excitation. Moreover, the dielectric-coated wire with current wave velocity less than c is treated. A closed-form solution is obtained for the rectangular pulse response.

II. General Field of a Straight Wire

Consider a transient traveling current wave on a straight wire (Fig. 1). Assume the current arises at point $z = a$ and is completely absorbed at $z = b$ after traversing the wire. If the wire is thin, the current wave can be modeled using

$$\vec{J}(\vec{r}, t) = \hat{z}\delta(x)\delta(y)I(t - z/v)\left[u(z - a) - u(z - b)\right] \tag{1}$$

where v is the wave velocity along the wire, $I(t)$ is the current waveform, and $u(t)$ is the unit step function. The retarded vector potential at an observation point in free space is then

$$\vec{A} = (\mu_0/4\pi)\int_V \frac{\vec{J}(\vec{r}', t - R/c)}{R}\, dv' \tag{2}$$

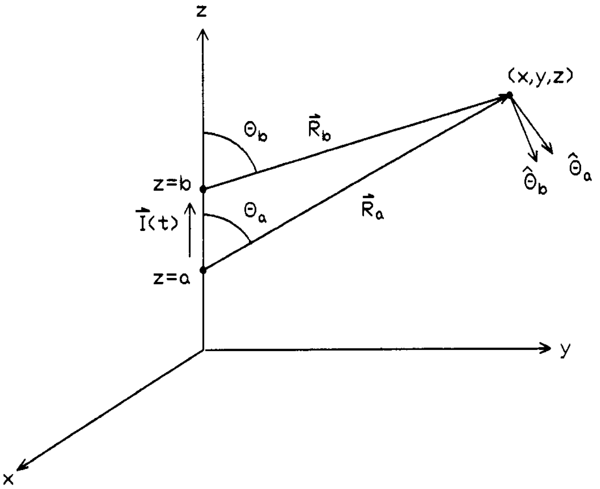

Fig. 1. Transient traveling current wave on a straight wire and local coordinate system.

where $R = |\vec{r} - \vec{r}'|$, whereas $\vec{A}$ is related to scalar potential ϕ through the Lorentz gauge

$$\nabla \cdot \vec{A} = -\mu_0\epsilon_0\, \partial\phi/\partial t. \tag{3}$$

The resulting electric field is

$$\vec{E} = -\nabla\phi - \partial\vec{A}/\partial t. \tag{4}$$

The field can be calculated using time-domain superposition. Replacing $I(t)$ with $\delta(t)$, the dirac delta function, gives the electric field impulse response $\vec{E}^h(\vec{r}, t)$. The field due to a general waveform $I(t)$ is then given by the convolution

$$\vec{E}(\vec{r}, t) = \int_{-\infty}^{t} I(t')\vec{E}^h(\vec{r}, t - t')\, dt'. \tag{5}$$

Using (2), the vector potential impulse response is calculated as

$$\vec{A}^h(\vec{r}, t) = (\mu_0/4\pi)\hat{z}\int_a^b \delta[G(z')]g(z')\, dz' \tag{6}$$

where $G(z') = t - z'/v - R/c$, and $g(z') = 1/R$. Making a change of variables $u = G(z')$ gives

$$A_z^h = -(\mu_0/4\pi)\int_{G(b)}^{G(a)} \delta(u)F[G^{-1}(u)]\, du \tag{7}$$

Manuscript received July 5, 1989; revised January 8, 1991.

E. J. Rothwell and P. Ilavarasan are with the Department of Electrical Engineering, Michigan State University, East Lansing, MI 48824.

M. J. Cloud is with the Department of Electrical Engineering, College of Engineering, Lawrence Technological University, Southfield, MI 48075.

IEEE Log Number 9144859.

0018-9375/91/0800-0172$01.00 © 1991 IEEE

where $F(z') = g(z')/G'(z')$, and $G'(z') = \partial G(z')/\partial z'$. This leads to

$$A_z^h = (\mu_0/4\pi)\begin{cases} -F[G^{-1}(0)] & \text{for } G(b) \leq 0 \leq G(a) \\ 0 & \text{otherwise} \end{cases} \tag{8}$$

where $G(a) = t - a/v - R_a/c$, $G(b) = t - b/v - R_b/c$, $R_a = [\rho^2 + (z-a)^2]^{1/2}$, and $R_b = [\rho^2 + (z-b)^2]^{1/2}$. (Note that ρ is the cylindrical coordinate radial variable.) Here, $G^{-1}(0)$ is the value z_0', which satisfies $G(z_0') = 0$, or

$$z_0' = (1/m^2)[(vt - n^2 z) \pm nD] \tag{9}$$

where $D^2 = (vt - z)^2 + \rho^2 m^2$, $m^2 = 1 - n^2$, and $n = v/c$. Substituting this value gives $F(z_0') = v/[-R_0 + n(z - z_0')]$, where $R_0 = R(z_0')$. Using $G(z_0') = t - z_0'/v - R_0/c = 0$ yields

$$F(z_0') = \pm v/D. \tag{10}$$

Since D is always positive, the minus sign must be chosen in (10) so that the vector potential (8) is in the same direction as the current. Putting (10) into (8) then gives the vector potential impulse response

$$\begin{aligned} A_z^h = (\mu_0 v/4\pi D)[&u(t - T_a - R_a/c) \\ &-u(t - T_b - R_b/c)] \end{aligned} \tag{11}$$

where $T_a = a/v$, and $T_b = b/v$. Note that the vector potential exists only within a time window dictated by the current wave transit time, and the propagation delay from the wire ends.

The scalar potential is determined by substituting (11) into (3). Taking care to properly evaluate step function derivatives results in the impulse response

$$\begin{aligned} \phi^h = \frac{\eta v}{4\pi}\Big((nD)^{-1} &- [n^{-1} - (z-a)/R_a] \\ &\cdot [(a + nR_a - z)^2 + \rho^2 m^2]^{-1/2}\Big) u(t - T_a - R_a/c) \\ &- \frac{\eta v}{4\pi}\Big((nD)^{-1} - [n^{-1} - (z-b)/R_b] \\ &\cdot [(b + nR_b - z)^2 + \rho^2 m^2]^{-1/2}\Big) u(t - T_b - R_b/c) \end{aligned} \tag{12}$$

where η is the free-space intrinsic impedance.

Using (11) and (12) in (4) gives the electric field impulse response

$$\begin{aligned} \vec{E}^h = &-\frac{\eta c}{4\pi} u(t - T_a - R_a/c)\left[m^2\left(\frac{\hat{R}_a[v(t-T_a)\cos\theta_a - R_a] - \hat{\theta}_a v(t-T_a)\sin\theta_a}{\{[v(t-T_a) - R_a\cos\theta_a]^2 + m^2 R_a^2 \sin^2\theta_a\}^{3/2}}\right) + \left(\frac{\hat{R}_a}{R_a^2}\right)\right] \\ &+ \frac{\eta c}{4\pi} u(t - T_b - R_b/c)\left[m^2\left(\frac{\hat{R}_b[v(t-T_b)\cos\theta_b - R_b] - \hat{\theta}_b v(t-T_b)\sin\theta_b}{\{[v(t-T_b) - R_b\cos\theta_b]^2 + m^2 R_b^2 \sin^2\theta_b\}^{3/2}}\right) + \left(\frac{\hat{R}_b}{R_b^2}\right)\right] \\ &+ \frac{\eta}{4\pi}\left[\hat{\theta}_a \delta(t - T_a - R_a/c)\left(\frac{n\sin\theta_a}{R_a(1 - n\cos\theta_a)}\right) - \hat{\theta}_b \delta(t - T_b - R_b/c)\left(\frac{n\sin\theta_b}{R_b(1 - n\cos\theta_b)}\right)\right]. \end{aligned} \tag{13}$$

Here, conversion from global to local coordinates is given through

$$\begin{aligned} \hat{z} &= \hat{R}_{a,b}\cos\theta_{a,b} - \hat{\theta}_{a,b}\sin\theta_{a,b} \\ \hat{\rho} &= \hat{R}_{a,b}\sin\theta_{a,b} + \hat{\theta}_{a,b}\cos\theta_{a,b} \end{aligned} \tag{14}$$

where $\sin\theta_a = \rho/R_a$, $\cos\theta_a = (z-a)/R_a$, $\sin\theta_b = \rho/R_b$, and $\cos\theta_b = (z-b)/R_b$. Finally, from (5), the general electric field is given by

$$\begin{aligned} \vec{E} = &+\frac{\eta}{4\pi}\left[\hat{\theta}_a I(t - T_a - R_a/c)\left(\frac{n\sin\theta_a}{R_a(1 - n\cos\theta_a)}\right) - \hat{\theta}_b I(t - T_b - R_b/c)\left(\frac{n\sin\theta_b}{R_b(1 - n\cos\theta_b)}\right)\right] \\ &- \frac{\eta c}{4\pi}\left(\hat{R}_a q(t - T_a - R_a/c)/R_a^2 - \hat{R}_b q(t - T_b - R_b/c)/R_b^2\right) \\ &- \frac{\eta c m^2}{4\pi}\int_{-\infty}^{t - T_a - R_a/c} I(t')\left[\frac{\hat{R}_a[v(t - T_a - t')\cos\theta_a - R_a] - \hat{\theta}_a v(t - T_a - t')\sin\theta_a}{\{[v(t - T_a - t') - R_a\cos\theta_a]^2 + m^2 R_a^2 \sin^2\theta_a\}^{3/2}}\right] dt' \\ &+ \frac{\eta c m^2}{4\pi}\int_{-\infty}^{t - T_b - R_b/c} I(t')\left[\frac{\hat{R}_b[v(t - T_b - t')\cos\theta_b - R_b] - \hat{\theta}_b v(t - T_b - t')\sin\theta_b}{\{[v(t - T_b - t') - R_b\cos\theta_b]^2 + m^2 R_b^2 \sin^2\theta_b\}^{3/2}}\right] dt' \end{aligned} \tag{15}$$

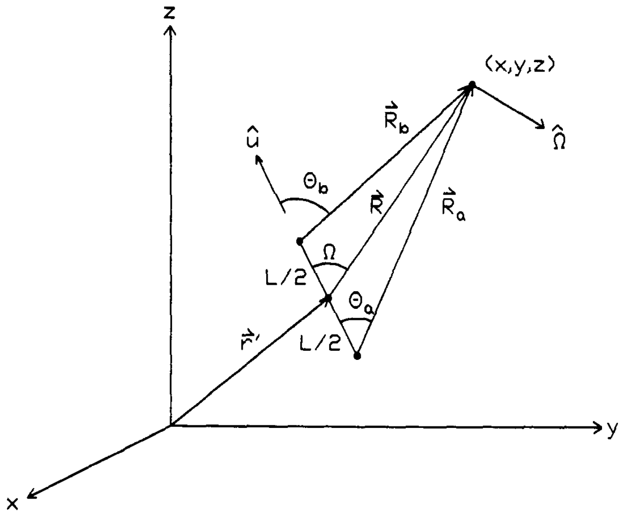

Fig. 2. Arbitrarily oriented wire and local coordinate system.

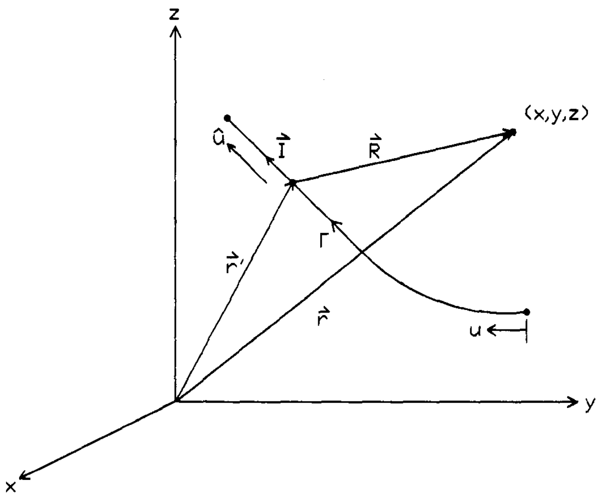

Fig. 3. General-shaped wire with traveling-wave current distribution.

where the charge q is given by $I = dq/dt$. It is interesting to note that when $v = c$ (i.e., the uncoated wire), this reduces to

$$\vec{E} = +\frac{\eta}{4\pi}\left[\hat{\theta}_a I(t - T_a - R_a/c)\left(\frac{n \sin\theta_a}{R_a(1 - n\cos\theta_a)}\right) - \hat{\theta}_b I(t - T_b - R_b/c)\left(\frac{n\sin\theta_b}{R_b(1 - n\cos\theta_b)}\right)\right]$$
$$- \frac{\eta c}{4\pi}\left(\hat{R}_a q(t - T_a - R_a/c)/R_a^2 - \hat{R}_b q(t - T_b - R_b/c)/R_b^2\right). \qquad (16)$$

These results are found to match previously published expressions. The $\hat{\theta}$ components in (16) are those furnished by Manneback [9], whereas the radial components match those in Schelkunoff [10].

III. FAR-ZONE SPECIALIZATION

The use of global coordinates in (15) allows the far-zone specialization for an arbitrarily oriented wire (Fig. 2). Neglecting terms that decrease faster than $1/R$, and using $R \gg L$, $\theta_a \cong \theta_b \cong \Omega$, $\hat{R}_a \cong \hat{R}_b \cong \hat{R}$, and $\hat{\theta}_a \cong \hat{\theta}_b \cong \hat{\Omega}$, gives

$$\vec{E}(\vec{r}, t) = (\eta/4\pi R)\hat{\Omega}F(\Omega)\left[I(t - T_0 - R_a/c) - I(t - T_0 - L/v - R_b/c)\right] \qquad (17)$$

where T_0 is the time at which the current wave enters the wire segment, and $F(\Omega) = n\sin\Omega/(1 - n\cos\Omega)$. Expanding the current functions in a Taylor series about $t - T_0 - R/c$ and using $\hat{u} = \hat{R}\cos\Omega - \hat{\Omega}\sin\Omega$, it is found that the leading terms cancel, whereas the second terms combine to give

$$\vec{E} = (\mu_0/4\pi)(L/R)\hat{R} \times (\hat{R} \times \hat{u})I'(t - T_0 - R/c) \qquad (18)$$

where $\hat{u}$ is the unit tangent to the straight wire, and higher-order terms can be neglected for a pulsewidth much larger than L/v.

IV. ARBITRARILY SHAPED WIRE

Treatment of a traveling-wave current distribution on an arbitrarily shaped wire (Fig. 3) uses (18) and superposition to give

$$\vec{E} = (\eta/4\pi c)\int_{\Gamma} \hat{R} \times \hat{R} \times \frac{\vec{I}'(t - u'/v - R/c)}{R}\,du' \qquad (19)$$

for a line current along curve Γ.

V. NUMERICAL RESULTS

The straight wire behavior can be best illustrated through numerical examples. The special case of a rectangular pulse current waveform yields a closed-form answer for $\vec{E}$ and is used in subsequent examples. Letting $I(t) = I_0[u(t) - u(t - \gamma)]$ in (15), and using

$$\beta_{a,b} = \begin{cases} 0 & \text{if } t - T_{a,b} - R_{a,b}/c < 0 \\ \gamma & \text{if } \gamma < t - T_{a,b} - R_{a,b}/c \\ t - T_{a,b} - R_{a,b}/c & \text{if } \gamma > t - T_{a,b} - R_{a,b}/c \end{cases} \qquad (20)$$

leads to

$$\vec{E} = (\eta/4\pi)\left(\hat{\theta}_a I(t - T_a - R_a/c)\frac{n\sin\theta_a}{R_a(1 - n\cos\theta_a)} - \hat{\theta}_b I(t - T_b - R_b/c)\frac{n\sin\theta_b}{R_b(1 - n\cos\theta_b)}\right)$$
$$- (\eta c/4\pi)I_0\left[\hat{R}_a\beta_a/R_a^2 - \hat{R}_b\beta_b/R_b^2\right]$$

$$
\begin{aligned}
&-(\eta c m^2/4\pi) I_0\{\hat{R}_a \sin^2\theta_a([n^2 R_a^2 v\cos\theta_a - R_a v^2(t-T_a)]/\Delta_a(t-T_a)\\
&-[n^2 R_a^2 v\cos\theta_a - R_a v^2(t-T_a-\beta_a)]/\Delta_a(t-T_a-\beta_a))\\
&-\hat{\theta}_a v\sin\theta_a([R_a v\cos\theta_a(t-T_a) - R_a^2(1-n^2\sin^2\theta_a)]/\Delta_a(t-T_a)\\
&-[R_a v\cos\theta_a(t-T_a-\beta_a) - R_a^2(1-n^2\sin^2\theta_a)]/\Delta_a(t-T_a-\beta_a))\}\\
&+(\eta c m^2/4\pi) I_0\{\hat{R}_b \sin^2\theta_b([n^2 R_b^2 v\cos\theta_b - R_b v^2(t-T_b)]/\Delta_b(t-T_b)\\
&-[n^2 R_b^2 v\cos\theta_b - R_b v^2(t-T_b-\beta_b)]/\Delta_b(t-T_b-\beta_b))\\
&-\hat{\theta}_b v\sin\theta_b([R_b v\cos\theta_b(t-T_b) - R_b^2(1-n^2\sin^2\theta_b)]/\Delta_b(t-T_b)\\
&-[R_b v\cos\theta_b(t-T_b-\beta_b) - R_b^2(1-n^2\sin^2\theta_b)]/\Delta_b(t-T_b-\beta_b))\}
\end{aligned}
\tag{21}
$$

where

$$
\Delta_{a,b}(t) = m^2 v^2 R_{a,b}^2 \sin^2\theta_{a,b}\{[vt - R_{a,b}\cos\theta_{a,b}]^2 + m^2 R_{a,b}^2 \sin^2\theta_{a,b}\}^{1/2}. \tag{22}
$$

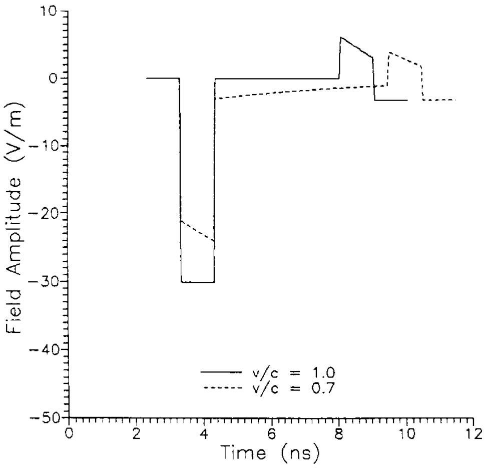

Fig. 4. Near-zone axial component of electric field in the $z = 0$ plane due to a straight wire on the z axis for $a = 0$, $b = 1$ m, $\rho = 1$ m, $\gamma = 1$ ns.

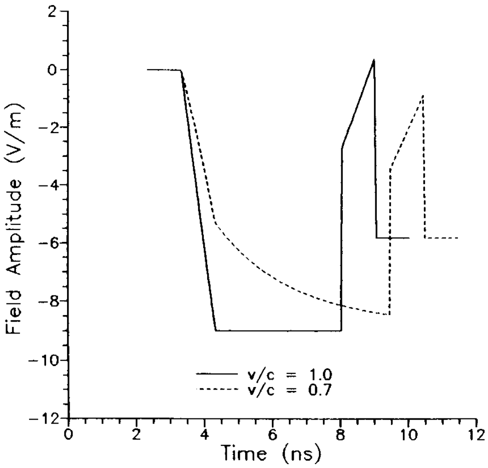

Fig. 5. Near-zone radial component of electric field in the $z = 0$ plane due to a straight wire on the z axis for $a = 0$, $b = 1$ m, $\rho = 1$ m, $\gamma = 1$ ns.

Figs. 4 and 5 show the near-zone axial (E_z) and radial (E_ρ) components of $\vec{E}(z = 0, t)$ caused by a straight wire on the z axis, computed using (21) with pulse duration $\gamma = 1$ ns (which is less than the wave transit time L/v along the wire). In this case, there is no $\hat{R}_a$-component contribution to the axial field. Thus, when $v = c$, the charge term in (15) is not implicated; the first axial field event exactly duplicates the current pulse, as is revealed by (15). This field originates when current appears at $z = a$. The second event seen when $v = c$ is due to current being absorbed at $z = b$; both transit time L/v and the path length difference from the wire ends account for the later starting time. Since both $\hat{\theta}_b$ and $\hat{R}_b$ contributions to the field exist, the pulse is not exactly duplicated. The slope visible here is due to the charge accumulation described in (15). The total accumulation remains as residual static charge; thus $\vec{E}$ remains constant and nonzero after the second event.

When $v \neq c$, the third term of (15) augments contributions from the current waveform; thus, the first event is not an exact duplicate of $I(t)$. This term accumulates; therefore, the second event merges into the first but begins later due to the greater transit time L/v. The same residual $\vec{E}$ results as with the $v = c$ case because v does not affect total charge accumulation.

The radial field component (Fig. 5) exhibits similar behavior. As E_ρ lacks a $\hat{\theta}_a$ component, when $v = c$ only the charge term contributes to (15); this is the leading edge of the field waveform. The constant slope is due to charge accumulating at $z = a$. When the current pulse has completely passed $z = a$, a constant field is maintained by accumulated charge until the current reaches $z = b$. Then, both $\hat{\theta}_b$ and $\hat{R}_b$ components contribute to E_ρ and form the second event in Fig. 5. A constant residual field remains after the end of the second event, which is caused by the total accumulated charge at both $z = a$ and $z = b$. When $v \neq c$, the constant $\vec{E}$ produced by charge accumulating at $z = a$ is augmented by the third term in (15); therefore, the first and second events merge.

Far-zone outcomes are shown in Figs. 6 and 7 for the same $I(t)$. Terms in E_ρ vary inversely with distance squared from the wire, whereas E_z has a term that varies inversely with distance; this accounts for the vertical scale difference between these two graphs. Each event in the axial field plot corresponds to the current wave passing a wire end and replicates $I(t)$. Due to decay of inverse-square terms, no residual field appears. The amplitude difference between the cases $v = c$ and $v \neq c$ is given by the ratio $n = v/c$ in (15).

The radial field is quite similar to its near-zone counter-

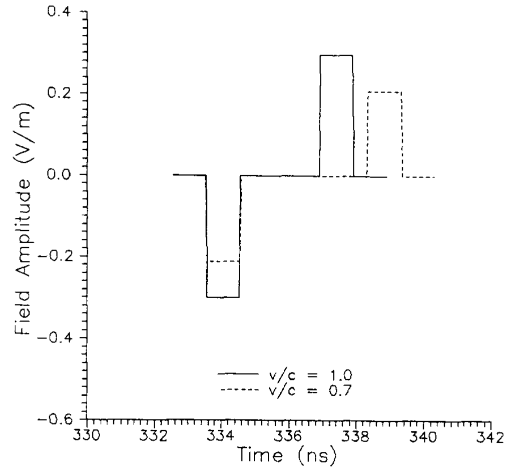

Fig. 6. Far-zone axial component of electric field in the $z = 0$ plane due to a straight wire on the z axis for $a = 0$, $b = 1$ m, $\rho = 100$ m, $\gamma = 1$ ns.

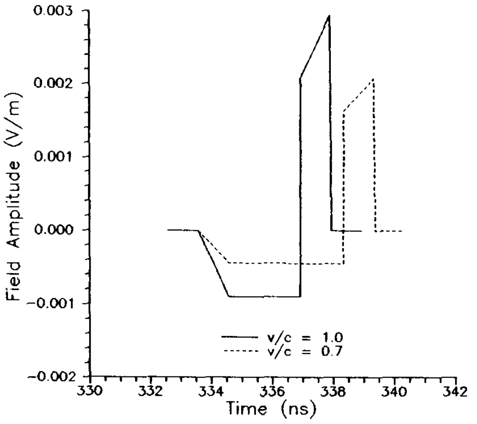

Fig. 7. Far-zone radial component of electric field in the $z = 0$ plane due to a straight wire on the z axis for $a = 0$, $b = 1$ m, $\rho = 100$ m, $\gamma = 1$ ns.

part. However, the effect of the accumulating term in (15) is reduced, and the two events are separate. It is interesting to note the absence of a residual field after the second event; radial component cancellation in the far-zone static fields is responsible.

VI. EXPERIMENTAL RESULTS

To verify the theory presented above, an experiment was performed using a straight-wire transmitting antenna located above a 20 × 32-ft aluminum ground plane. The antenna was fabricated as an extension of the center conductor of a 50 Ω coaxial cable with the outer conductor contacting the ground plane. The antenna was fed by a Picosecond Pulse Labs model 1000B-01 pulse generator, providing quasirectangular pulses of 1-ns duration and amplitude 40 V (Fig. 8). The radiated waveform was then measured using a 2.4-cm monopole probe coupled to a Tektronix 7854 waveform processing oscilloscope via $S2$ sampling heads (75-ps risetime). Proper timing was accomplished using the variable trigger delay internal to the pulse generator. One hundred waveforms were measured during each experiment and averaged in real time, using a pulse repetition rate of 1000 kHz, and transferred via a general-purpose-interface bus to an IBM PC microcomputer for analysis and plotting (see [12] for a complete schematic of the experimental setup).

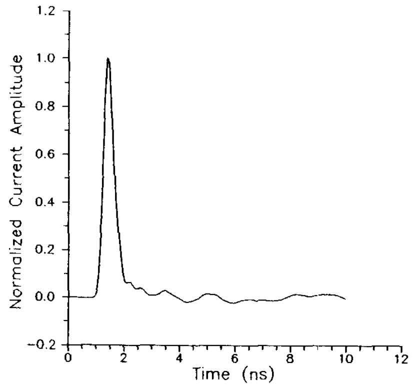

Fig. 8. Experimental current pulse waveform.

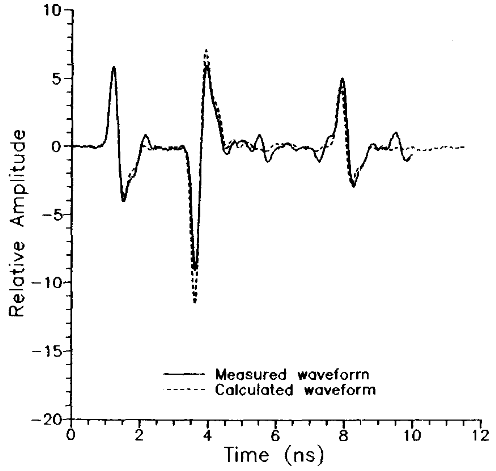

Fig. 9. Near-zone axial field (measured and theoretical) for 63.5 cm uninsulated wire measured at $\rho = 2.49$ m, $z = 0$.

The feeding mechanism used in the experiment provides a useful means for testing the theory presented in this paper. Since the current waveform appears instantaneously from the coaxial aperture onto the wire, (1) is an appropriate model as long as the current induced on the ground plane is replaced by a downward traveling current wave using the method of images. Similarly, when the current wave reaches the end of the wire, it is instantaneously reflected back toward the feed and thus can be decomposed into an upward traveling wave disappearing at the top of the wire and a downward traveling wave arising from the same point. Thus, the current distribution on the wire can be represented as a superposition of distributions of the form (1).

Figure 9 shows the near-zone axial field measured by the monopole for an uninsulated transmitting antenna of length 63.5 cm. Because the short probe acts as a differentiator, the waveform in Fig. 9 is actually the time derivative of E_z. The

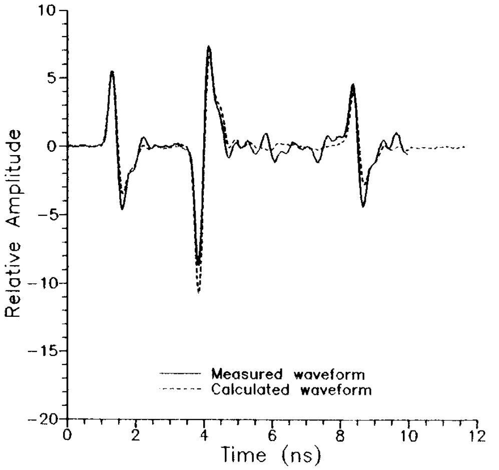

Fig. 10. Near-zone axial field (measured and theoretical) for 63.5 cm insulated wire measured at $\rho = 2.49$ m, $z = 0$.

first event originates when current is introduced at the wire bottom and replicates the current pulse derivative. The second event is produced by current reflecting from the wire end. The reflection coefficient is seen to be negative; therefore, the fields induced by the wire and its image add. When the reflected current wave returns to the feed point, it is re-reflected but with a positive coefficient. In this case, the wire and image fields cancel; only a small event is seen. The third event is created by the second reflection from the wire end. The significant difference between field amplitudes generated by the first and second reflections is due to radiation loss. These results are quite similar to those observed by Schmitt *et al.* [13], using a similar experimental setup.

The dotted line shown in Fig. 9 represents the time derivative of theoretical $\vec{E}$, computed using (15). Here, $I(t)$ is the pulse shown in Fig. 8, whereas the propagation velocity is found experimentally to be $v = 0.992$ c. The theoretical curve is developed by superimposing straight-wire solutions with current and wave directions chosen to match the multiple reflections of the antenna/image system. The reflection coefficient at the antenna end is taken to be -1 for the first reflection and 0 for the second reflection; at the feed, $+1$ is used. The theory agrees quite well with experiment.

Similar results are shown in Fig. 10 for an insulated wire transmitting antenna. Here, the reflections occur at later times than with the uninsulated wire; thus, $v < c$. The dotted line in Fig. 10 shows the theoretical curve corresponding to $v = 0.931$ c. Again, good agreement is attained.

VII. A Directive Time-Domain Antenna

As an example of radiation by a curved wire, consider the proposed directive time-domain antenna shown in Fig. 11. Here, a two-wire transmission line is perturbed in the $x-y$ plane according to the equation

$$y = \pm lA\left[1 - \cos\left(2\pi x/l\right)\right] \tag{23}$$

where l is antenna length along the x direction. The antenna

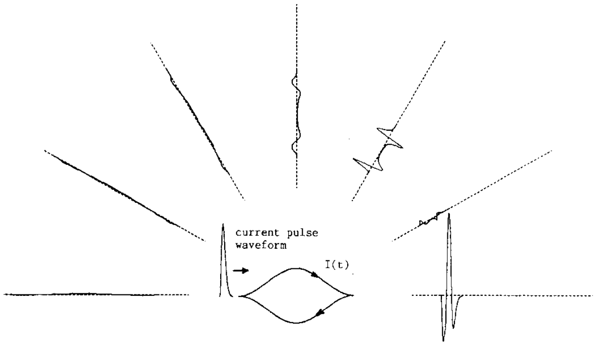

Fig. 11. Raised-cosine time-domain antenna and circumferential component of its far-zone field in the $z = 0$ plane.

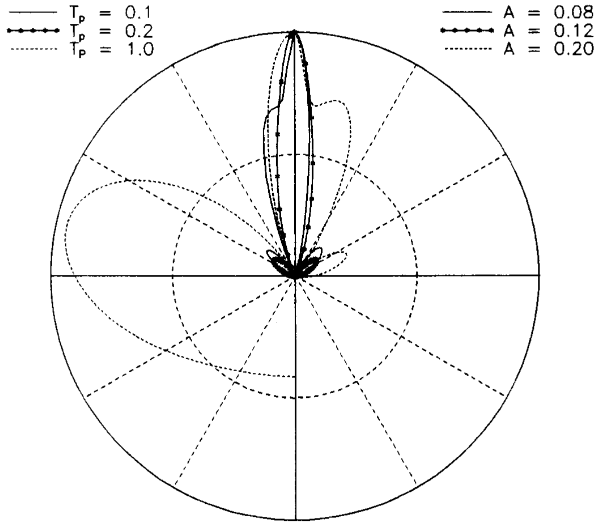

Fig. 12. Energy in the waveform radiated by the raised-cosine antenna as a function of azimuth angle for (left) $A = 0.12$ and (right) $T_p = 0.2$.

is excited by a transmission line current pulse

$$I(t) = \tau^2\left[e^{-6\tau} - e^{-7\tau}\right] \tag{24}$$

traveling with $v = c$ along the wire, where

$$\tau = (2t/T_p)(c/l) \tag{25}$$

with T_p representing a selectable normalized pulse width.

Figure 11 also shows the circumferential ($\hat{\phi}$) component of the far-zone field in the x-y plane as a function of azimuth angle ϕ, calculated using (19). The antenna radiates most strongly along $\phi = 0°$. It is found that the combination of $A = 0.12$ and $T_p = 0.2$ provides optimum directionality of energy in the radiated waveform. This is seen in Fig. 12, which shows the radiated waveform energy for various choices of antenna width A and pulse width T_p. When A is decreased from 0.12, the main lobe width decreases, but the sidelobe near $\phi = 50°$ increases substantially. When A is increased from 0.12, main lobe width increases dramatically. If T_p is made smaller than 0.1, both main lobe width and sidelobe height increase. If T_p is made larger, a significant sidelobe develops, which also produces large amounts of radiation along the backward direction.

This type of directive time-domain antenna has two important benefits over more typical antennas. First, since the antenna is nonresonant (i.e., the far-end reflection is removed to any desired distance by adding transmission line), it radiates wide-band waveforms. Second, the smooth wire shape limits current waveform dispersion to that produced by radiation with minimal continuous reflection along the curved path [14].

VIII. Conclusion

This paper presents a time-domain theory for the transient fields produced by a general traveling-wave current on a straight wire antenna. A closed-form solution for a rectangular-pulse current waveform is revealed; numerical results from this permit the investigation of the differences between near versus far zones and coated versus uncoated wires. Experimental findings for both coated and uncoated wires show good agreement with theory.

The results are also used to reach an expression for the far-zone field of a general curved wire; this facilitates investigation of radiation from a proposed narrowbeam transient antenna. It is shown that for properly chosen pulse width, the antenna can be made quite directive.

References

[1] H. F. Harmuth and S. Ding-Rong, "Antennas for nonsinusoidal waves. I. Radiators," *IEEE Trans. Electromagn. Compat.*, vol. EMC-25, pp. 13-24, Feb. 1983.

[2] H. Shen, R. W. King, and T. T. Wu, "Theoretical analysis of the rhombic simulator under pulse excitation," *IEEE Trans. Electromagn. Compat.*, vol. EMC-25, pp. 47-55, Feb. 1983.

[3] N. Zaiping, "Radiation characteristics of traveling-wave antennas excited by nonsinusoidal currents," *IEEE Trans. Electromagn. Compat.*, vol. EMC-25, pp. 24-31, Feb. 1983.

[4] R. H. Bates and G. A. Burrell, "Towards faithful radio transmission of very wide bandwidth signals," *IEEE Trans. Antennas Propagat.*, pp. 684-690, Nov. 1982.

[5] G. Franceschetti and C. Papas, "Pulsed antennas," *IEEE Trans. Antennas Propagat.*, pp. 651-661, Sept. 1974.

[6] E. Miller and J. Landt, "Direct time-domain techniques for transient radiation and scattering from wires," *Proc. IEEE*, pp. 1396-1423, Nov. 1980.

[7] L. Marin, "Transient radiation from a resistive, tubular antenna," *Radio Sci.*, vol. 9, pp. 631-638, June 1974.

[8] Z. Chen, "Theoretical solutions of transient radiation from traveling-wave linear antennas," *IEEE Trans. Electromagn. Compat.*, vol. EMC-30, pp. 80-83, 1988.

[9] C. Manneback, "Radiation from transmission lines," *AIEE J.*, vol. 42, pp. 95-105, Feb. 1923.

[10] S. Schelkunoff, *Advanced Antenna Theory*. New York: Wiley, 1952.

[11] D. Sengupta and C. Tai, "Radiation and reception of transients by linear antennas," in *Transient Electromagnetic Fields* (L. Felson, Ed.) New York; Springer-Verlag, 1976, pp. 181-235.

[12] N. Gharsallah, E. Rothwell, K. M. Chen, and D. P. Nyquist, "Identification of the natural resonance frequencies of a conducting sphere from a measured transient response," *IEEE Trans. Antennas Propagat.*, pp. 141-143, Jan. 1990.

[13] H. J. Schmitt, C. W. Harrison, and C. S. Williams, "Calculated and experimental response of thin cylindrical antennas to pulse excitation," *IEEE Trans. Antennas Propagat.*, pp. 120-127, Mar. 1966.

[14] G. A. Burrell, "Propagation of current on bent wire antennas-An experimental study," *IEEE Trans. Antennas Propagat.*, pp. 427-434, May 1978.

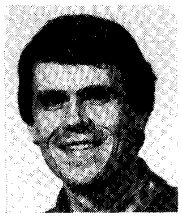

Edward J. Rothwell (S'84-M'85) was born in Grand Rapids, MI, on September 8, 1957. He received the B.S. degree in electrical engineering from Michigan Technological University, Houghton, in 1979, the M.S. degree in electrical engineering and the degree of electrical engineer from Stanford University, Stanford, CA, in 1980 and 1982, and the Ph.D. degree in electrical engineering from Michigan State University, East Lansing, in 1985, where he held the Dean's Distinguished Fellowship.

He worked for Raytheon Co., Microwave and Power Tube Division, Waltham, MA, from 1979-1982 on low-power traveling wave tubes and for MIT Lincoln Laboratory, Lexington, MA, in 1985. He has been at Michigan State University from 1985-1990 as an assistant professor of electrical engineering and from 1990 as an associate professor. His research interests include radar target identification and transient electromagnetic theory.

Dr. Rothwell is a member of Phi Kappa Phi.

Michael J. Cloud (M'88) was born in Grand Rapids, MI, on December 30, 1960. In 1983, he received the B.S. degree with high honor in electrical engineering from Michigan State University, East Lansing. He received the M.S. and Ph.D. degrees in electrical engineering from Michigan State University in 1985 and 1987, respectively, where he held the Dean's Distinguished Fellowship.

Since 1987, he has been Assistant Professor of Electrical Engineering at Lawrence Technological University, Southfield, MI.

Dr. Cloud is a member of Sigma Xi, Golden Key, and Phi Kappa Phi.

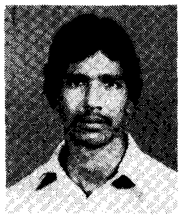

Ponniah Ilavarasan was born in Puloly, Sri Lanka, on July 27, 1962. He received the B.S. and M.S. degrees in electrical engineering from Michigan State University, East Lansing, in 1986 and 1988, respectively. He is currently working toward the Ph.D. degree in electromagnetics at Michigan State University.

His current topics of interest are developing and implementing an efficient scheme in radar target discrimination using E/S pulses.

Mr. Ilavarasan is a member of Eta Kappa Nu.